The Astrophysical Journal, 623:866–876, 2005 April 20

WARM MOLECULAR GAS TRACED WITH CO $J = 7 \rightarrow 6$ IN THE GALAXY'S CENTRAL 2 PARSECS: DYNAMICAL HEATING OF THE CIRCUMNUCLEAR DISK

C. M. Bradford,[1] G. J. Stacey, and T. Nikola
Department of Astronomy, Cornell University, 610 Space Sciences Building, Ithaca, NY 14853

A. D. Bolatto
Department of Astronomy and Radio Astronomy Laboratory, University of California, 601 Campbell Hall, Berkeley, CA 94720-3411

J. M. Jackson
Institute for Astrophysical Research, Boston University, 725 Commonwealth Avenue, Room 514, Boston, MA 02215

and

M. L. Savage and J. A. Davidson
USRA SOFIA, NASA Ames Research Center, Moffet Field, CA 94035
Received 2004 September 4; accepted 2005 January 2

ABSTRACT

We present an 11″ resolution map of the central 2 pc of the Galaxy in the CO $J = 7 \rightarrow 6$ rotational transition. The CO emission shows rotation about Sgr A* but also evidence for noncircular turbulent motion and a clumpy morphology. We combine our data set with available CO measurements to model the physical conditions in the disk. We find that the molecular gas in the region is both warm and dense, with $T \sim 200-300$ K and $n_{H_2} \sim (5-7) \times 10^4$ cm^{-3}. The mass of warm molecular gas we measure in the central 2 pc is at least 2000 $M_\odot$, about 20 times the UV-excited atomic gas mass, ruling out a UV heating scenario for the molecular material. We compare the available spectral tracers with theoretical models and conclude that molecular gas is heated with magnetohydrodynamic shocks with $v \sim 10-20$ km s^{-1} and $B \sim 0.3-0.5$ mG. Using the conditions derived with the CO analysis, we include the other important coolants, neutral oxygen and molecular hydrogen, to estimate the total cooling budget of the molecular material. We derive a mass-to-luminosity ratio of $\sim$2–3 $M_\odot L_\odot^{-1}$, which is consistent with the total power dissipated via turbulent decay in 0.1 pc cells with $v_{rms} \sim 15$ km s^{-1}. These size and velocity scales are comparable to the observed clumping scale and the velocity dispersion. At this rate, the material near Sgr A* is dissipating its orbital energy on an orbital timescale and cannot last for more than a few orbits. Our conclusions support a scenario in which the features near Sgr A* such as the circumnuclear disk and northern arm are generated by infalling clouds with low specific angular momentum.

Subject headings: Galaxy: center — Galaxy: nucleus — ISM: molecules — turbulence

Online material: color figure

1. INTRODUCTION

The Galactic center provides the opportunity to study many of the fascinating phenomena associated with massive black holes and galactic nuclei in the greatest detail. The region is likely similar to the nuclei of galaxies beyond the Milky Way, particularly those harboring low-luminosity active galactic nuclei (LLAGNs) with similar sub-Eddington luminosities. Since the Galactic center radio and infrared sources were first discovered decades ago (Oort & Rougoor 1960; Becklin & Neugebauer 1968, 1969; Balick & Brown 1974), the central source and its circumnuclear material have been the subject of intense study from infrared to radio frequencies using both continuum and spectroscopic probes.

In the radio continuum, the central few parsecs show a spiral-like structure of thermal emission, termed the minispiral or Sgr A West, roughly centered on the bright, nonthermal point source Sgr A* (Ekers et al. 1983; Lo & Claussen 1983). The arms of the radio minispiral are interpreted as the ionized remains of tidally disrupted infalling clouds, a notion supported by the large ($\sim$500 km s^{-1}) velocity dispersion in the ionized gas observed via mid-IR fine-structure and radio recombination lines (Lacy et al. 1980; Schwarz et al. 1989). The distribution of molecular and neutral atomic gas shows a different morphology: interferometric observations of HCN show a substantial portion of an inclined ringlike structure of diameter approximately 3 pc surrounding Sgr A*, with kinematic evidence for rotational motion of about 110 km s^{-1} around the center (Güsten et al. 1987; Wright et al. 1989). In contrast, the neutral oxygen emission shows a peak inside the circumnuclear ring but also shows general evidence of rotational motion in the same sense as the HCN (Jackson et al. 1993, hereafter J93).

The first far-IR observations demonstrated that the substantial IR luminosity (few times 10^6 $L_\odot$) at the center of the galaxy is due to dust absorbing UV and optical energy and reradiating it at longer wavelengths (Hoffman et al. 1971; Gatley et al. 1977; Gatley & Becklin 1981). Subsequent mapping revealed bilobal structure with temperature decreasing with distance from the center, suggesting a circumnuclear ring or disk around a central 2–3 pc evacuated cavity containing the primary luminosity source (Becklin et al. 1982).

[1] Current address: Jet Propulsion Laboratory, California Institute of Technology, Mail Stop 169-507, Pasadena, CA 91109; matt.bradford@jpl.nasa.gov.

The far-IR, radio continuum, and molecular features have been unified with high-resolution far-IR images (Latvakoski et al. 1999, hereafter L99). Far-IR images at 31 and 38 μm provide color temperature, optical depth, and luminosity maps of the inner 2×3 pc region, trace the deposition of UV luminosity, and constrain the masses of the features. The most prominent feature is the circumnuclear disk (CND) itself. Here the far-IR typically peaks 1″–3″ (0.03–0.1 pc) farther from Sgr A* than the radio continuum (e.g., Sgr A West), and the molecular gas ring as traced with HCN has a larger radius still. This is as would be expected in a typical photodissociation region (PDR) situation in which the progression from the UV source is ionized gas traced with radio continuum (photodissociated gas and warm dust) molecular gas. Given the similarity in the morphology and kinematics of the radio arcs, the far-IR ring, and the HCN ring, a plausible scenario is therefore that these features trace different aspects of the same structure, a ring or torus of material orbiting the central mass, called the CND.

In addition to the CND, the other prominent features distinctly traced in both the far-IR and radio are the northern arm (NA) and the east-west bar, both part of the radio source identified as SGR A West. The radio continuum and far-IR morphologies again make a nice match, and their kinematics as probed via the radio recombination lines suggests that these features are distinct infalling streamers on parabolic orbits around Sgr A*. The neutral oxygen emission ([O I]) was originally attributed to material within the cavity formed by the CND (J93) but has been shown to be primarily originating from the NA itself. The sizes and column densities as traced with the dust continuum imply average gas densities of $(1.6–4) \times 10^4$ cm^{-3}, consistent with the average densities derived for the atomic gas (10^4–10^5 cm^{-3}).

Aside from a few local heating sources, the color temperature map of the region presented by L93 is strongly peaked in the center near Sgr A*, and the run of temperature with radius follows the same $T \sim r^{-0.4}$ law across all of the features. The central cluster massive young He I stars centered within an arcsecond of Sgr A* (collectively called IRS 16), in concert with the other stellar clusters, thus make an appealing mechanism for centrally ionizing and heating the material in the CND and the other streamers (L99).

While the UV sources near Sgr A* are thus a good explanation for the warm dust and atomic gas in the NA and the inner edge of the CND, UV photons are not necessarily the heating source of the molecular material that comprises the bulk of the CND. Various theoretical models for the formation of the CND invoke infalling clouds and require cloud-to-cloud collisions (Vollmer & Duschl 2002; Sanders 1998). Dynamical heating has been suggested as a mechanism for molecular clouds in the Galaxy's central 500 pc to explain bright rotational H_2 lines (Rodríguez-Fernández et al. 2000, 2001) and the presence of highly excited NH_3 (Wilson et al. 1982; Herrnstein & Ho 2002). At the position of Sgr A* itself, the rovibrational molecular hydrogen lines show an almost completely thermal spectrum, much like the Orion KL shock (Tanaka et al. 1989; Gatley et al. 1986), demonstrating that UV is not responsible for the heating of this warm molecular gas.

Thus, the following question remains open: what are the relative roles of the dynamical and ultraviolet energy sources in exciting the molecular gas in the central 2 pc? More generally, what is the origin, lifetime, and eventual fate of this material? To address these questions, we have mapped the $J = 7 \rightarrow 6$ rotational transition of carbon monoxide (CO) in this region. The mid-J CO rotational transitions are especially useful probes for the Galactic center because they are thermalized and optically thick in the circumnuclear disk but suffer little extinction and virtually no line optical depth in the foreground Galactic material. We use CO lines to estimate the mass and conditions of the warm molecular gas. We trace more than 2000 $M_\odot$ and derive a moderate density, $n \sim (2–7) \times 10^4$ cm^{-3}, and warm temperature, $T \sim 200–300$ K. Unlike the atomic gas and the warm dust traced in the far-IR continuum, the bulk of this warm molecular component is likely heated dynamically via magnetohydrodynamic (MHD) shocks due to clump-clump collisions, not UV photons from the central sources.

The observations are described in § 2. In § 3 we present the results of our CO observations and a brief comparison with the morphological and kinematic features observed in other tracers. (We will present a more detailed morphological study using a larger, higher spatial resolution map in a subsequent article.) Analysis of the CND molecular gas excitation is presented in § 4, and a discussion of the CND gas heating mechanism follows in § 5.

2. OBSERVATIONS

The CO $J = 7 \rightarrow 6$ ($\nu = 806.65$ GHz) observations were made in 1999 April at the James Clerk Maxwell Telescope (JCMT) on the commissioning run of the submillimeter Fabry-Perot spectrometer SPIFI. Details of the instrument and its performance can be found in Bradford et al. (2002). In its first-light configuration, the detector array included 12 bolometers, arranged on an incomplete 4×4 grid with 8″ spacing. Over the two nights, the array was placed in 11 positions, 6 of which included sufficient field rotation to warrant being split into two pointings, generating a total of 17 independent pointings of the array. Each pointing is comprised of 30–50 spectral scans of the Fabry-Perot with the telescope nodded every two scans to exchange the source and reference beams. For these observations, the velocity resolution of the spectrometer was 70 km s^{-1}, and the total scan bandwidth was 620 km s^{-1}. The spectra were sampled at 50 km s^{-1}, but the data are rebinned at a finer resolution to allow proper co-adding of the various pixels around the array, each of which has a small relative velocity shift.

Calibration was based on Mars, which was near opposition and was taken to be a uniform disk of size 15.″8 and brightness temperature 201 K, the mean of the models of Wright (1976) and Rudy et al. (1987). At the time of the observations, the forward coupling of the telescope was measured to be 0.65, of which 8.5% coupled to Mars. This low value of the coupling to Mars resulted from a combination of telescope surface and misfigured reimaging lenses. On subsequent observing runs this coupling was measured to be ~20%, consistent with other observations at 800 GHz.

All Galactic center observations were conducted in submillimeter band 2 weather ($\tau_{225} > 0.05$). When combined with the low elevation of the source, this provided a transmission to the source between 0.03 and 0.10. The atmospheric transmission for each scan was determined with the 225 GHz radiometer according to

$$\tau_{806\ \mathrm{GHz}} = 37(\tau_{225\ \mathrm{GHz}} - 0.012). \quad (1)$$

This relation was calibrated by measuring sky emission against an ambient load as a function of zenith angle and comparing the derived opacity to the measured 225 GHz opacity. With the low telescope coupling and atmospheric transmission, the system noise-equivalent flux density for the observations was $\sim 3 \times 10^{-21}$ ergs s^{-1} cm^{-2} Hz^{-1} Hz$^{-1/2}$.

Once the 12 spectra are generated from each pointing, the total flux for each pixel in each pointing is calculated by integrating over -160 km s$^{-1} < v < 160$ km s^{-1}, to provide adequate baseline and trace the same gas as with HCN and NH_3. The overlaps in the various pointings then allow for determining the appropriate scalings between the various pointings; these relative scalings are as much as a factor of 1.8 over the entire set of 17 pointings, but the scaling does not change by more than 30% between two pointings adjacent in time.

The spectra were then mosaicked together by regridding onto a uniform 0.″43 spatial by 10 km s^{-1} spectral grid. At a given velocity, T_{MB} in each pixel is determined by any surrounding data points as follows: Each observed point is placed into the spatial array as a delta function with magnitude equal to its intensity. The map is generated by smoothing this array with an 11″ Gaussian kernel, then normalizing each position by a template map obtained by the same smoothing of an array with unity at each data point. With the incompletely filled array and the effects of field rotation some regions of the map are highly sampled, while others are very sparse; thus, the sensitivity in the map varies substantially. For a typical interior point in the map, there are between one and three spectra per beam, and we estimate the relative uncertainty to be ~300 K km s^{-1} from beam to beam, and about twice this value across the entire map, the additional error accumulating as a result of the mosaicking together of several pointings. The map boundaries are defined to be where the template array drops below 0.4, that is, where there is not a single observed point within 6″; thus, large regions near the map boundaries may be influenced only by a small number of observed points. The overall calibration uncertainty is estimated to be about 30%, owing to the varying atmospheric conditions during the observations and calibration.

3. RESULTS

The integrated intensity map in CO $J = 7 \rightarrow 6$ of the central 2 pc is presented in Figure 1, along with five spectra of various positions offset from Sgr A*. Emission is observed throughout the $2' \times 1'$ mapped region, with a minimum integrated intensity of 900 K km s^{-1} (referred to the main-beam temperature). The peak in the CO emission is in the southwest, likely part of the CND, with an intensity of 5400 K km s^{-1}, and the average intensity throughout the region is 2550 K km s^{-1}. In this section we first compare our results with previous observations of the same tracer. We then compare our map with high-resolution maps in the far-IR continuum and the density tracer HCN in order to address the morphology and kinematics of the warm-CO–containing gas. Hereafter we adopt a distance of 7.9 ± 0.3 kpc to the Galactic center, according to the analysis of McNamara et al. (2000).

3.1. *Comparison with Previous Observations*

The integrated intensities we measure are somewhat lower than those of Harris et al. (1985), who observed CO $J = 7 \rightarrow 6$ in nine 30″ beams offset in Galactic longitude from Sgr A*. Harris et al. (1985) do not present a two-dimensional map, but their brightest observed position is toward the southwest part of the CND with a total measured luminosity of 200 $L_\odot$ in the 30″ beam. Integrating over a 30″ beam centered on the peak in our map results in only 105 $L_\odot$.

A potential explanation for this discrepancy is self-chopping in our observation. We employed a 120″ chop in right ascension, the maximum usable for efficient operation at the JCMT. With this chop the reference beam does approach the "+20 km s^{-1}" and "+50 km s^{-1}" Sgr A clouds, large extended clouds lying roughly 1′–3′ to the east of Sgr A* (Genzel et al. 1990). Genzel et al. (1990) have observed these objects in CO $J = 7 \rightarrow 6$ with roughly eight 30′ pointings, finding peak intensities around 600–800 K km s^{-1}, over large (~1′) regions. Harris et al. (1985) were able to use a 190″ chop throw on the Infrared Telescope Facility, which clears the majority of the Sgr A clouds. While the chopping onto these clouds is thus a difference between our observations and those of Harris et al. (1985), the effect is not likely to account for the significant difference in observed intensities. Because we were nodding the telescope, exchanging between an eastern and a western reference beam, the error introduced by an 800 K km s^{-1} source in one of the reference beams is at most ~400 K km s^{-1}, or ~10% of the observed flux density. Our spectra show no obvious indication of reference beam emission, and a comparison of our primary data set with a small sample data set obtained using a 90″ chop does not show any evidence of reference beam emission affecting the map. Apart from the overall calibration difference, our map corresponds well with the large-beam pointings of Harris et al. (1985), in both relative integrated flux and velocity spread of the emission across the region.

Moneti et al. (2001) present a single $J = 7 \rightarrow 6$ spectrum toward Sgr A*, obtained with the Caltech Submillimeter Observatory (CSO); their data show an integrated intensity of 700 K km s^{-1} in T_A^*. Taking a main-beam efficiency of 0.3, as in our measurements with the JCMT, this corresponds to a main-beam intensity of 2330 K km s^{-1}, 64% of the 3650 K km s^{-1} we measure. Our measurements are therefore intermediate between the other published values, which vary by a factor of more than 2.

3.2. *Morphology and Kinematics*

CO $J = 7 \rightarrow 6$ emission is detected throughout our observed region. We reserve the detailed kinematic and morphological study for the higher spatial resolution, larger area data set presented in a subsequent paper. For the purposes of this study, we simply overlay the CO data set on the 38 μm continuum image (L99) in Figure 2 and the interferometric HCN map (Güsten et al. 1987) in Figure 3. We highlight two points, which lead to the conclusions that the gas tracing the mid-J CO bears some relation but is not identical to the CND material traced with HCN or the high-excitation NH_3:

1. The bright CO emission peak in the southwest is coincident with the far-IR peak at the same location: (−15, −30). This location corresponds to a smaller radius (1.2 pc projected) but the same position angle as the HCN peak. The bright CO emission 20″–30″ south of Sgr A* is similar to that found in the map of NH_3 (6, 6), tracing molecular gas at a few hundred kelvins (Herrnstein & Ho 2002). We note that with our moderate spatial resolution and relatively small coverage, the CO and NH_3 maps do not agree in detail, as the NH_3 peak is farther east. In general, both tracers show that warm gas is interior to the circumnuclear ring as traced with HCN.

2. Kinematically, the warm CO shows evidence of motion about Sgr A*. The spectra in Figure 1 reveal a clear north-south velocity gradient with the same sense of rotation as is observed in the HCN. However, the CO $J = 7 \rightarrow 6$ does not show the obvious ring shape, nor the well-organized circular orbit of the dense gas traced with the HCN. Neglecting the morphological asymmetry, the observed orbital velocity of ~60 km s^{-1} line of sight (65 km s^{-1} deprojected with 67° inclination), at a distance of 35″, suggests an interior mass of only 1.3×10^6 $M_\odot$. This is substantially less than the mass traced with HCN and

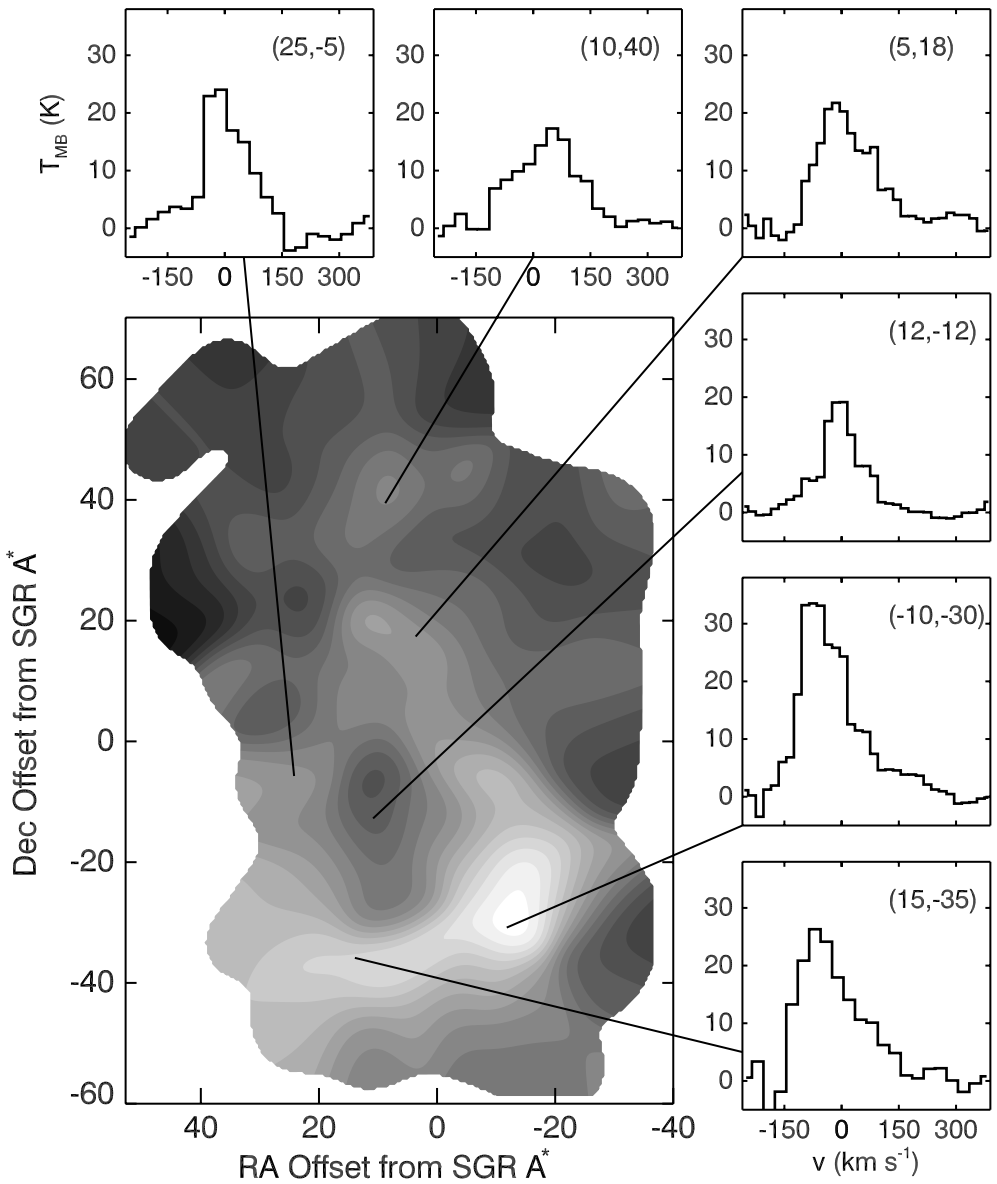

FIG. 1.—Integrated intensity map of the CO $J = 7 \rightarrow 6$ emission from the Galactic center CND. Offsets are relative to Sgr A* (R.A.$_{B1950.0} = 17^h42^m29^s.3$, decl.$_{B1950.0} = -28^\circ59'19''$), and the beam size is $11''$ FWHM. Emission is observed throughout the map; contours are linear in $T_{MB}\Delta v$, with a 250 K km s^{-1} interval. The peak in the southwest CND is 5400 K km s^{-1}; the minimum at the edges of the map is 750 K km s^{-1}. Velocity resolution in the spectra is 70 km s^{-1}. Overall rotational motion is evident in the shifting of the velocity from north to south.

dramatically less than the central dark mass traced with the stellar velocity field ($M \sim 4.0 \times 10^6\ M_\odot$; Ghez et al. 2003; Schödel et al. 2003). Evidently, the CO-containing gas does not have angular momentum for a stable orbit at its distance from the central mass. Herrnstein & Ho (2002) reached a similar conclusion in their mapping of NH_3 (6, 6). Again aside from this general similarity, the two tracers do not share detailed kinematics: the CO shows a sense of rotation similar to that of the HCN, while the NH_3 does not.

4. PHYSICAL CONDITIONS IN THE GALACTIC CENTER MOLECULAR GAS

Bright CO $J = 7 \rightarrow 6$ emission implies the presence of both warm and dense gas. The $J = 7$ level lies 155 K above ground and the $J = 7 \rightarrow 6$ transition has a high critical density, $n_{crit} = 4 \times 10^5$ cm^{-3} for thermalization. Our peak brightness temperature of 33 K originates in gas with a minimum physical temperature of $T = (h\nu/k)[\ln(h\nu/kT_{MB} + 1)]^{-1} = 51$ K, if the transition were optically thick, thermalized, and filled the $11''$ beam. This is a strong lower limit: in reality the gas is at lower density and does not fill the beam, which requires a higher temperature.

4.1. *Large Velocity Gradient Radiative Transfer Calculations*

We combine our $J = 7 \rightarrow 6$ observations with published CO observations in the far-IR ($J = 14 \rightarrow 13$ and $J = 16 \rightarrow 15$; Lugten 1987) and millimeter ($J = 2 \rightarrow 1$ and $J = 1 \rightarrow 0$; Serabyn et al. 1986) to estimate the conditions in the molecular gas in the framework of a large velocity gradient (LVG) radiative transfer model. The code calculates intensities of the rotational CO lines up to $J = 18 \rightarrow 17$, given a molecular hydrogen density, temperature, and velocity gradient in km s^{-1} pc^{-1}. The process was originally employed for the study of molecular

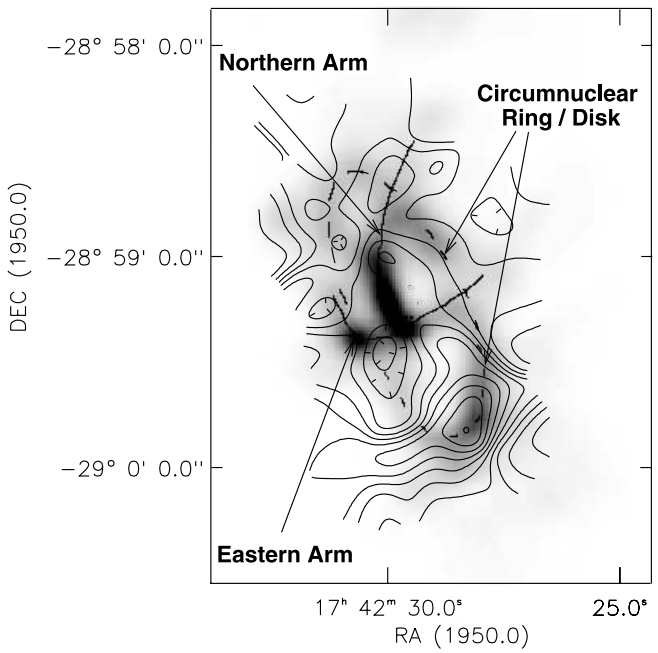

FIG. 2.—CO $J = 7 \rightarrow 6$ contours overlaying the gray-scale far-IR continuum image of L99, which shows the morphological features around Sgr A*. The southwest peak in CO is coincident with the far-IR peak in the southwest CND, while the CO ridge to the north lies between the NA and the northwest CND. The extension of the NA to the north is clearly detected in CO. CO contours are in units of $T_{\rm MB}\Delta v$, peaking at 5400 K km s^{-1}, with an interval of 375 K km s^{-1}.

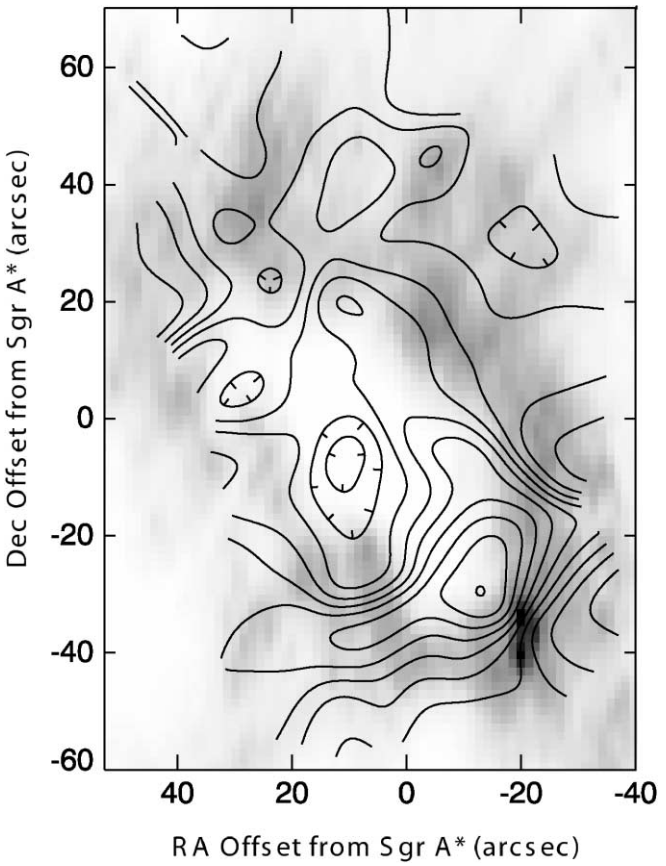

FIG. 3.—CO $J = 7 \rightarrow 6$ contours overlaying the gray-scale interferometric HCN $J = 1 \rightarrow 0$ map (R. Güsten & M. C. H. Wright 2000, private communication). CO generally peaks interior to the HCN but shows the same clumpy structure in the northern CND. The gap in the HCN ring to the north corresponds to the extension of the NA as traced in CO. CO contours are as in Fig. 2. [*See the electronic edition of the Journal for a color version of this figure.*]

clouds by Scoville & Solomon (1974) and Goldreich & Kwan (1974), and further description of the model used here can be found in Bradford et al. (2003). As in their study of the nuclear molecular gas in NGC 253, we adopt a velocity gradient much larger than the traditional values of a few kilometers per second per parsec appropriate only for cool, quiescent molecular clouds in the disk of the Milky Way. For the material in the central 2 pc, we take dv/dz to be 300 km s^{-1} pc^{-1}, consistent with our observed velocity width of $\sim$100 km s^{-1} in an 11″ beam. We adopt 8×10^{-5} for $X_{\rm CO}$, the CO fractional abundance relative to H_2. This value is intermediate between that inferred from observations of the massive Galactic clouds Sgr B2 and Orion IRc2 (for which $X_{\rm CO} \sim 6 \times 10^{-5}$; Leung et al. 1984; Evans et al. 1991) and that of chemical models (for which $X_{\rm CO} \sim 1.5 \times 10^{-4}$; e.g., Blake et al. 1987). Collisional rates are from Flower (2001) and D. R. Flower (2004, private communication), increased by 21% to account for collisions with helium (McKee et al. 1982; Viscuso & Chernoff 1988; Flower & Launay 1985; Schinke et al. 1985).

For a meaningful run of line intensity with J, all observed intensities are averaged over a 44″ beam corresponding to the far-IR beam size. This average beam is centered toward the $J = 7 \rightarrow 6$ peak in the southwest at $(-15, -30)$. Figure 4 shows the constraints imposed by two line ratios. We use the $J = 16 \rightarrow 15$ to $J = 7 \rightarrow 6$ and $J = 7 \rightarrow 6$ to $J = 2 \rightarrow 1$ ratios, as these straddle the peak in the run of intensity versus J. The thick contours correspond to observed ratios, and their intersection region represents the range of possible solutions. With errors on the submillimeter and far-IR intensities estimated at 30%, the line ratios should be considered good to $\sim$40%, admitting a large range of solutions over which temperature can be traded with density. It is clear that the temperature is greater than 200 K and that the molecular hydrogen density is less than 10^5 cm^{-3}, although there are no stringent upper limits on the temperature using the available rate coefficients. We favor temperatures toward the lower end of the allowed range shown in Figure 4 because of the lack of evidence for higher temperature molecular tracers, as discussed in § 4.3. Given this constraint, we plot a suitable solution ($n_{\rm H_2} = 7.1 \times 10^4$ cm^{-3}, $T = 240$ K) superposed on the observed line intensities in Figure 5. In this model, τ exceeds unity for $J_{\rm upper} = 7-10$ but does not exceed 2 owing to the LVG appropriate in the CND. Our conclusions for the southwest CND are inconsistent with the conditions reported by Moneti et al. (2001) for the gas toward Sgr A* itself: $T \sim 250$ K and $n_{\rm H_2} \sim 3 \times 10^5$ cm^{-3}. We deduce smaller densities, in spite of using the same collisional rates from Schinke et al. (1985). All of our inferences are based on a fit to the observations toward the peak of the CO emission in the southwest CND. It is possible that the molecular gas is more highly excited toward Sgr A* itself than in the southwest CND, although distinguishing between the two is difficult given the large beams for the high-J far-IR lines. Based on the 50″ resolution *Infrared Space Observatory* (*ISO*) maps of Sgr A* in CO $J = 14 \rightarrow 13$ (White et al. 1999), we estimate that the CO line ratios are similar throughout the region, suggesting similar excitation conditions in the gas. If so, the discrepancy may arise from our LVG that should be applicable given the dynamics of the region, which allows the $J = 7$ transition to radiate more efficiently and with lower collisional excitation than in more optically thick models.

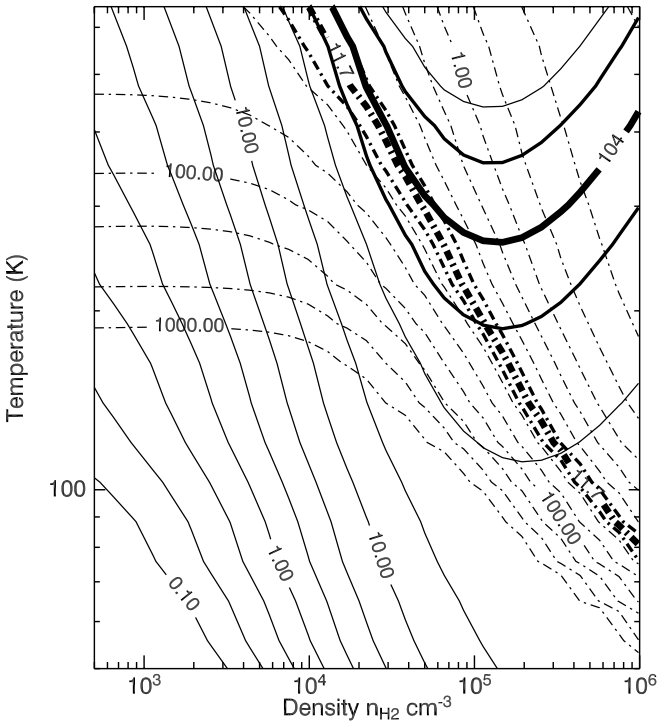

FIG. 4.—LVG constraints for the gas in the CND. Two line ratios are plotted: $J = 7 \rightarrow 6$ to $J = 2 \rightarrow 1$ (*solid lines*) and $J = 7 \rightarrow 6$ to $J = 16 \rightarrow 15$ (*dashed lines*). Thick lines correspond to observed values in the SW CND; the two medium-weight lines for each ratio show the range allowed by the 40% uncertainty. Calculations assume a velocity gradient of 300 km s^{-1} pc^{-1} (see text), and the temperature range reflects the availability of CO-H_2 collisional rate coefficients.

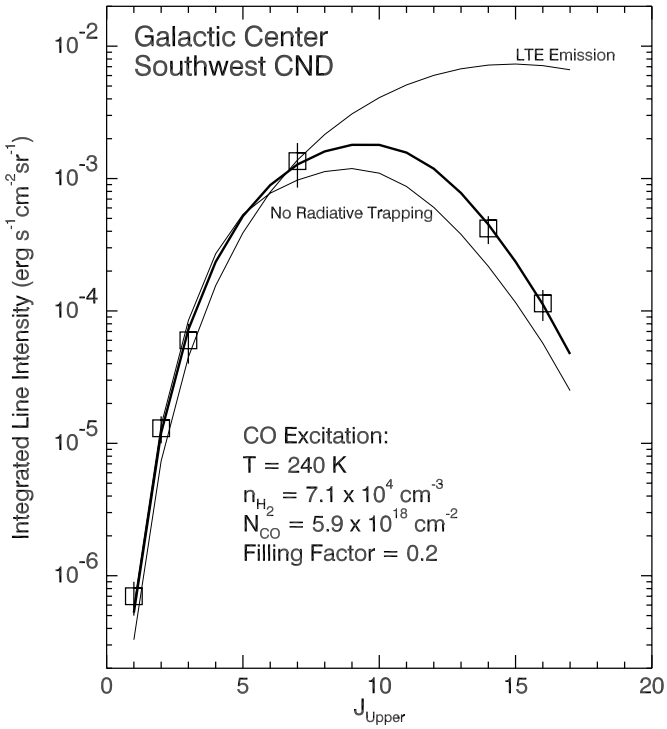

FIG. 5.—Model of the excitation and radiative transfer of CO using an LVG, escape probability approximation. Observed intensities are averaged over a 44″ beam centered at (δR.A. = −15″, δdecl. = −30″) from Sgr A*. CO $J = 7 \rightarrow 6$ is from this work, the other points from Lugten (1987), Serabyn et al. (1986), and Sutton et al. (1990). Error bars are conservative at 30%, reasonable for the calibration uncertainties in the submillimeter and far-IR lines, but likely an overestimate of the uncertainty in the lower J lines. The lighter curves demonstrate intensities that would be generated in LTE and without including the effects of radiative excitations of the upper levels.

4.2. *Molecular Gas Mass, Clumping*

Using the model plotted in Figure 5, the required CO column density is $N_{CO} = 1.2 \times 10^{18}$ cm^{-2} in the 44″ beam, or $N_{H_2} = 1.5 \times 10^{22}$ cm^{-2} with our assumed CO abundance of 8×10^{-5}. The 44″ represents 2.2 pc^2, and total molecular gas mass in this beam is therefore 530 $M_\odot$. If the excitation conditions are similar throughout our mapped region, then we can scale the column density with the observed $J = 7 \rightarrow 6$ intensity. In this case, the beam-averaged column density in a beam toward Sgr A* itself is ∼60% of our peak value and is 6 times that reported by Moneti et al. (2001). This discrepancy is difficult to reconcile. It could be due in part to the larger CSO beam relative to our JCMT observations, although this effect is unlikely given that our map shows extended emission.

More fundamentally, even if the $J = 7 \rightarrow 6$ transition were optically thin and thermalized, it would be impossible to generate the observed emission toward the peak in our map with the CO column density reported by Moneti et al. (2001). On the other hand, our analysis could be consistent with a larger CO column given the lack of any optically thin mid-J CO isotopic transitions. Other analyses of cooler material suggest somewhat larger molecular column densities. For example, J93 compile low-J CO, CS, and HCN measurements and infer $N_{H_2} = 4 \times 10^{22}$ to 4×10^{23} cm^{-2}, in 10″–30″ beams toward the southwest CND. They suggest that the HCN emission comes from very dense ($n_{H_2} = 10^6$–10^8 cm^{-3}) material, distributed with low beam filling factor in small clumps. While our analysis indicates that this density is not appropriate for the material that produces the bulk of the mid-J CO emission, it is possible that clumps at these high densities could harbor molecular gas that could be locally optically thick and thus inefficient in contributing to the total CO emission. Again, we stress that our model employs a higher temperature and larger velocity gradient, both of which allow the CO to radiate more efficiently than previously considered. Thus, our mass and column density estimates should be considered as lower limits to the total warm molecular gas mass. Finally, we note that our analysis is not sensitive to cool gas that does not radiate in the high-J lines, and a cool component could exist along with the warm one we measure. Such a two-component molecular medium (25% at 200 K, 75% at 25 K) has been proposed based on the high-J NH_3 observations of Galactic center clouds (Huettemeister et al. 1993; Herrnstein & Ho 2005).

Scaling the mass in the 44″ beam to the entire map using the CO $J = 7 \rightarrow 6$ intensity yields a mass of $\sim 2 \times 10^3$ $M_\odot$ as a lower limit to the warm molecular gas in the central 2 pc. Comparing the total mass with the derived density implies a volume filling factor of 4.4×10^{-2} and an area filling factor of 0.12 in the 44″ beam. This filling factor is reasonable: it is approximately equal to the product of the filling factor of the overall ring shape as observed at the 11″ resolution in the 44″ beam used for the calculations and the intrinsic clumpiness in the ring on scales below our 11″ beam.

The size of the clumps is not constrained with the large-beam analysis. At a maximum, all of the 530 $M_\odot$ of gas is in a single 0.6 pc diameter clump, corresponding to $A_V = 138$ mag. The facts that we are resolving the ring shape in our 11″ beam and that the HCN and far-IR maps show clumping at the limit of their resolution (4″–12″ = 0.15–0.46 pc) suggest that material is clumped on smaller scales (L99; Güsten et al. 1987; Wright

TABLE 1
GALACTIC CENTER ISM TRACERS

PARAMETER	GALACTIC CENTER			ORION OMC 1	
	Sgr A*[a]	Northern Arm (25″)[b]	Southwest CND (25″)[b]	Bar PDR[c]	KL Shock[c]
O I 63 μm	2.1×10^{-2}	4.1×10^{-2}	2.3×10^{-2}	4.0×10^{-2}	2.7×10^{-2}
O I 145 μm	$8. \times 10^{-4}$	(1)	(0.93)	3.5×10^{-3}	3.0×10^{-3}
C II 158 μm	1.7×10^{-3}	(1)	(1)	4.2×10^{-3}	3.5×10^{-3}
C I 609 μm	$4. \times 10^{-5}$	...	...	...	...
CO $J = 1 \rightarrow 0$	$7. \times 10^{-7}$	$7. \times 10^{-7}$	$7. \times 10^{-7}$	$4. \times 10^{-7}$	2.7×10^{-6}
CO $J = 7 \rightarrow 6$	8×10^{-4}	1.1×10^{-3}	1.5×10^{-3}	3×10^{-4}	9×10^{-3}
CO $J = 14 \rightarrow 13$	1.7×10^{-4}	...	...	3.1×10^{-4}	8.6×10^{-3}
Far-IR continuum ratios	22	50	26	26	390

[a] Intensity (ergs s^{-1} cm^{-2} sr^{-1}) averaged over a 2′ diameter beam around Sgr A*. The far-IR line intensities are taken from J93 and Genzel et al. (1985), the CO $J = 7 \rightarrow 6$ from this work, and the CO $J = 1 \rightarrow 0$ from Serabyn et al. (1986). The far-IR continuum is from the luminosity maps of L99 and includes a contribution of 30% from the warm transiently heated dust grains, which are not traced by the 32–38 μm continuum. All intensities are corrected for extinction toward the Galactic center, for which we take $\tau = 23.5\lambda[\mu\mathrm{m}]$ after L99.

[b] Average intensities over 25″ beams, for tracers with sufficient angular resolution, units and references as above. Relative intensities in the two regions for tracers with larger ($\sim$1′) beams are given in parentheses, estimated from the *ISO* LWS maps of White et al. (1999). (R.A., decl.) offsets from Sgr A*: northern arm, (+5″, +15″); southwest CND, (−15″, −30″).

[c] Intensities in $\sim$1′ regions centered on the far-IR bar, and the BN-KL object of Orion. References are Herrmann et al. (1997), Schmid-Burgk et al. (1989), Stacey et al. (1993), and Watson et al. (1985).

et al. 2001). A clump size of order 0.2 pc might be expected on physical grounds, as it is comparable to the Jeans length scale, over which self-gravity becomes important,

$$L_{\mathrm{J}} = \left(\frac{kT}{mG\rho_m}\right)^{1/2} \sim 0.2 \text{ pc} \qquad (2)$$

for the cooler conditions inferred from the CO lines, $T = 200$ K and $n_{\mathrm{H_2}} = 7 \times 10^4$ cm^{-3}. With this size, the 44″ beam harbors 25 clumps, each with a mass of 22 $M_\odot$, and the clump column density corresponds to $A_V = 47$. This is sensible in a scenario in which clumpy molecular material is falling toward Sgr A* from greater distance, but is not tenable in the context of steady-state motion about Sgr A* at the CND radius. Any clump with density less than $n_{\mathrm{H_2}} \sim 6 \times 10^7$ cm^{-3} is Roche unstable in the presence of the tidal forces of the central mass concentration. Thus, any clumps associated with the material emitting CO are most likely transient structures.

4.3. *Molecular Gas Luminosity*

The CO excitation model provides a good estimate of the mass and total cooling due to CO in the molecular gas. The above fit to the data corresponds to a total emergent intensity in the CO lines of 1.5×10^{-2} ergs s^{-1} cm^{-2} sr^{-1} averaged over the 44″ modeled region. This intensity is substantial, comparable to that of the far-IR atomic fine-structure lines (see Table 1), and about 0.1% of the integrated dust continuum intensity. The modeled column density corresponds to a mass density of 7.05×10^{-2} g cm^{-2}, and assuming that the CO lines radiate isotropically, we derive a mass-to-luminosity ratio of $L_{\mathrm{CO}}/M_{\mathrm{H_2}} = 1.4\, L_\odot\, M_\odot^{-1}$ for the CO cooling around Sgr A*.

For a complete energy budget of the warm molecular gas, we now consider the other coolants. Detailed chemical studies indicate that in addition to CO, the most important cooling paths for densities above 10^3 cm^{-3} and temperatures above 150 K are the rotational transitions of H_2 and H_2O and the fine-structure lines of atomic oxygen ([O I]; Goldsmith & Langer 1978; Neufeld et al. 1995 and references therein). In what follows, we estimate the efficiency of these coolants and conclude that, for the conditions we derive with our LVG analysis, it is likely that CO, H_2, and [O I] contribute comparably to the cooling budget.

The quadrupole H_2 lines have low radiative rates and are thus optically thin and thermalized at our modeled densities. The cooling per gram is then easily estimated using (for details see Le Bourlot et al. 1999)

$$\frac{L}{M} = \sum_J \frac{f_u A_{u,l} h\nu}{1.43\,(2m_p)}, \qquad (3)$$

where f_u is the fraction in the upper level, given by Boltzmann's equation, and η_{op} is the ortho–to–para ratio. The rotational H_2 lines are thermalized for densities above 10^4 cm^{-3}, and the combined ortho and para cooling function is not strongly dependent on the η_{op} for $T > 100$ K. With $T = 240$ K and $\eta_{\mathrm{op}} = 3$, the most important line is the $J = 3 \rightarrow 1$, which produces $0.29\, L_\odot\, M_\odot^{-1}$. All of the H_2 lines combined generate $\sim$0.41 $L_\odot$ $M_\odot^{-1}$ at this temperature, some 30% of the CO cooling. We do note that the H_2 lines become much more efficient coolants as the temperature increases. For $T = 325$ K, the H_2 line cooling becomes comparable to our measured CO cooling, and any moderate-density ($n < 10^6$ cm^{-3}), high-temperature regions will be cooled primarily by the H_2 lines.

As the density increases, the oxygen-bearing species O, O_2, and H_2O become important. Because the oxygen elemental abundance ($\sim 3 \times 10^{-4}$) is larger than that of carbon ($\sim 1.4 \times 10^{-4}$; Savage & Sternbach 1996), there is atomic and molecular oxygen in the UV-shielded cloud interiors where all the gas-phase carbon is locked up in CO. The chemical models for warm molecular gas (e.g., Neufeld et al. 1995) predict O^0 and O_2 abundances relative to H_2 of 1×10^{-4} (each) for $T < 250$ K. As the temperature increases to $\sim$500 K, all of the oxygen not locked in CO is likely in the form of H_2O; its contribution is described below. Since O_2 is not an important coolant owing to its lack of a strong dipole, we only need to consider the fine-structure transitions of [O I], and of the two, only the $J = 1 \rightarrow 0$ 63 μm is energetically important. The upper level of the 63 μm transition lies 228 K above ground and would thus be well populated given the molecular gas temperature if not for the high density required to thermalize the transition,

$n_{\rm crit} = 8 \times 10^5 (100/T[{\rm K}])^{0.69}$ cm^{-3} $= 4.4 \times 10^5$ cm^{-3}. Neglecting the upper ($J = 0$) level, we can model an emergent intensity under a two-level approximation:

$$I_{[\rm O\ I]\ 63\ \mu m} \sim \frac{h\nu N_{\rm O} A}{4\pi} \left[\frac{(g_u/g_l) e^{-h\nu/kT}}{1 + (g_u/g_l) e^{-h\nu/kT} + (n_{\rm crit}/n)} \right] = 1.0 \times 10^{-2} \text{ ergs s}^{-1} \text{ cm}^{-2} \text{ sr}^{-1}, \quad (4)$$

where g_u and g_l are the statistical weights, $A = 9 \times 10^{-5}$ s^{-1}, and we have taken the temperature and density from the CO analysis. We have assumed that the emission is optically thin, which is reasonable given the large velocity dispersion of the warm molecular gas:

$$\tau = \frac{c^3 A N_{\rm O}}{8\pi\nu^3 \Delta v} \left[\left(1 + \frac{n_{\rm crit}}{n}\right) e^{h\nu/kT} - 1 \right] \times \left[\frac{(g_u/g_l) e^{-h\nu/kT}}{1 + (g_u/g_l) e^{-h\nu/kT} + (n_{\rm crit}/n)} \right] = 0.25. \quad (5)$$

Correcting for extinction and averaging the [O I] maps of J93 over the 44″ beam toward the southwest peak, White et al. (1999) obtain an intensity of 2.4 ergs s^{-1} cm^{-2} sr^{-1} (see § 4.4). In this region, therefore, the neutral oxygen present in the molecular gas produces nearly half of the observed [O I] 63 μm emission and represents 70% of the total cooling in the CO lines. Evidently the neutral oxygen plays an important role in cooling this warm dense molecular gas, and much of the observed [O I] should be attributed to the molecular phase, not the atomic gas.

For very warm molecular gas $T > 300$ K, H_2O becomes an important molecular coolant. Chemical models predict an H_2O abundance relative to H_2 as high as 3×10^{-4} as the temperature increases to 500 K, as it is the dominant oxygen repository under these conditions. Once formed through the chemical network, there are several far-IR rotational transitions of H_2O, and their radiative rates are fast because of the molecule's large dipole moment. For densities sufficient to thermalize these transitions, they will therefore dominate the cooling of the gas. The critical densities, however, are of order a few times 10^5 cm^{-3}, larger than the density inferred with the CO lines. For the gas we observe, both the temperature and the density of the gas are thus insufficient to generate and excite H_2O substantially, and it is not likely a major contributor to the cooling budget. Recent observations with the *Odin* satellite confirm that the cooling is small: ~60 K km s^{-1} in the 557 GHz ($1_{1,0} \rightarrow 1_{0,1}$) in the 2.′1 diameter beam (Sandqvist et al. 2003). Taking the warm gas to fill the beam gives a lower limit to the intensity of 1.1×10^{-5} ergs s^{-1} cm^{-2} sr^{-1}, about 80 times less than the CO $J = 7 \rightarrow 6$ line. If all this flux is referred to the 44″ beam used in the CO analysis, the integrated intensity would be 8.3×10^{-5} cm^{-3}, which represents a generous upper limit but is still 10 times smaller than the observed CO $J = 7 \rightarrow 6$ line.

Furthermore, shorter wavelength H_2O lines observed with the *ISO* LWS are only found in absorption from foreground cold gas in the continuum (none of the profiles show evidence for emission with intensities comparable to the CO lines; Moneti et al. 2001) and therefore rule out a large amount of gas with temperatures higher than $T \sim 250$ K.

The theoretical modeling and the observational evidence therefore support the following cooling budget for the warm molecular gas if it is at the modeled temperature and density: the CO lines account for half of the total cooling, the [O I] 63 μm line one-third, and the H_2 rotational lines one-sixth. The total corresponds to a mass-to-luminosity ratio of 2.7 $L_\odot\ M_\odot^{-1}$. As discussed above, for any material at higher temperatures the H_2 and H_2O lines will become more efficient at cooling the gas, and the total molecular gas cooling will substantially increase.

4.4. *Relationship with the Atomic Gas*

In order to understand the relationship between the atomic and molecular interstellar medium (ISM) phases, it is necessary to distinguish between the morphological features in the central 2 pc. Estimates of the mass of atomic gas by J93 were based on their model fits to the [O I] and [C II] intensities toward the peak 25″ northeast of Sgr A*. Most of this emission is now believed to come from the NA, a tidally stretched infalling streamer that is dynamically distinct from the rest of the circumnuclear material (L99; Roberts et al. 1996). The dust optical depth in the NA corresponds to a hydrogen column density of $N_{\rm H} \sim (0.7\text{–}1.3) \times 10^{22}$ cm^{-3} (in the 4″–6″ far-IR beams), corresponding to an ultraviolet attenuation of only 2–4 mag through the streamer, insufficient to shield the bulk of the material from photodissociation. This optical depth, together with the proximity to the UV sources, makes the NA the dominant feature in the atomic tracers, but it is negligible in the overall mass budget of the molecular material in the central 2 pc.

By comparison, the dust emission toward the molecular peaks in the southwest CND is associated with cooler but much more massive structures. The optical depths in the clumps in the ring are an order of magnitude greater than in the NA, in general sufficient to shield the UV from the bulk of the material. As discussed in § 4.3, the warm molecular material as probed with the CO emission is responsible for much of the [O I] emission observed toward the southwest ring. The other half arises in the atomic component. To estimate the atomic gas mass fraction, we use the [O I] map to scale the mass estimate of J93 for the NA to the atomic fraction in the southwest CND peak. Including the extinction correction for J93, they estimate $N_{\rm H} = 1.2 \times 10^{22}$ cm^{-2} based on an intensity of 5.0×10^{-2} ergs s^{-1} cm^{-2} sr^{-1} (22″ beam). The $\sim 2.0 \times 10^{-2}$ ergs s^{-1} cm^{-2} sr^{-1} observed in the 44″ multiplied by 0.5 to remove the molecular gas component then scales to an atomic gas column of $N_{\rm H,SW\ atomic} \sim 2.4 \times 10^{21}$ cm^{-2}. Taking this southwest peak as indicative of the rest of the overall region, we conclude that the atomic gas makes a small contribution to the total mass: ~8% of that of the warm molecular material.

A plausible scenario is that the molecular gas and atomic gas are physically associated and coexist as different phases in the same morphological structures (e.g., clumps in the ring), as has been proposed by Genzel et al. (1985) and J93. For clumps illuminated from one side (as for a centrally heated region centered on Sgr A*), the fraction of photodissociated material is estimated by the ratio of the extinction in a typical PDR layer ($A_{V,\rm PDR} \sim 4$) to the extinction through the full clump. The fiducial 0.2 pc clumps/streamers discussed above would have $A_V = 47$; thus, for such structures, the mass ratio of the photodissociated surface layer to the bulk is consistent with the mass ratio based on the intensities.

5. HEATING OF THE MOLECULAR GAS

Having estimated the conditions and total cooling of the molecular gas in the Galaxy's central 2 pc, we turn now to its heating source. There are two potential mechanisms: photoelectric heating by UV photons, and dynamical heating. Both are a priori plausible near Sgr A*, given its intense UV sources and turbulent dynamical structure. Morphological evidence suggests that UV heating may be important. Warm CO peaks interior to

the HCN ring, in general, and at the same position as the far-IR emission in the southwest ring. The emission observed toward the north of Sgr A* may also be associated with the NA as it enters the cavity. Furthermore, the emission in [Si II], [C II], and the far-IR continuum requires UV heating, and the maps in these tracers are generally well explained in the context of $\sim 10^7\ L_\odot$ of visible–UV luminosity, most from near Sgr A*, illuminating dense clumps and streamers (L99).

However, a scenario that *only* involves UV photons exciting the molecular gas is difficult to support quantitatively. The intensity of the CO $J = 7 \rightarrow 6$ transition relative to the atomic lines and far-IR continuum is much larger than can be accounted for with any existing PDR model. The standard plane-parallel PDR models (Tielens & Hollenbach 1985; Kaufman et al. 1999) predict mid-J CO emission arising from a layer between $A_V \sim 3$ and $A_V \sim 7$: at $A_V \lesssim 3$ CO is photodissociated, and at $A_V \gtrsim 7$ the UV does not produce the heating necessary to excite these transitions. These models predict a [O I] 63 μm/CO $J = 7 \rightarrow 6$ ratio, R, between 600 and 1200 (Kaufman et al. 1999), nearly 2 orders of magnitude higher than our observed $R \sim 15$. The Orion Bar PDR presents a similar problem to the theory, although not as extreme, with $R \sim 130$ (Stacey et al. 1993). Clumpy models have been generated in attempts to explain the discrepancy (Burton et al. 1990; Meixner & Tielens 1993; Koester et al. 1994), and Burton et al. (1990) find that the Orion PDR intensities can be reasonably well modeled (to within factors of 2) as a mixture of clumpy PDRs, including some clumps with very high densities ($n = 10^7$ cm^{-3}). Unlike in the Orion PDR, however, a model that incorporates a large fraction of the gas at high density is not supported for Sgr A*, given the drop-off in CO line intensity above $J \sim 10$. The best clumpy PDR model of Burton et al. (1990) for Sgr A* based on the atomic lines, CO lines, and molecular hydrogen lines underestimates the CO $J = 7 \rightarrow 6$ line intensity by a factor of 25. The root of the problem is the fact that there is $\sim$15 times more warm molecular gas than atomic gas, geometrically impossible for a UV-heated medium. On this basis we rule out UV heating as a viable method for all but a small fraction of the warm molecular gas we observe. Rodríguez-Fernández et al. (2001, 2004) reach a similar conclusion in their study of H_2 rotational line emission from other Galactic center clouds.

5.1. *Shock Conditions in the Central* 2 pc

We conclude that dissipation of supersonic turbulence in shocks is a more likely source for heating the warm molecular material in the central 2 pc. Dynamical heating has been proposed in explaining the emission from rotational H_2 lines in Galactic center clouds (Rodríguez-Fernández et al. 2004), and the presence of SiO in these clouds suggests a chemical history that includes shocks (Huettemeister et al. 1998).

Various models for the origin and dynamics of the features around Sgr A* have been constructed (e.g., Vollmer & Duschl 2002; Sanders 1998), which include infalling clouds and clump-clump collisions. The presence of clumps that are not Roche stable in the CND supports the notion that molecular material feeds into the central parsecs and that dynamical effects are important. Observations of molecular hydrogen provide further evidence: the molecular hydrogen rovibrational lines observed toward the northeast and southwest CND show a spectrum that is almost completely thermal, very much like the Orion shock (Tanaka et al. 1989; Gatley et al. 1986). Qualitatively, the spectral tracers around Sgr A* show some similarity to the shock region in Orion (BN-KL), with very bright CO lines relative to all other tracers, [O I], [C II], and the continuum (see Table 1). As indicated by the high-J lines, however, the shock conditions in the bulk of the Galactic center gas are clearly less intense than the Orion KL shock, where the CO emission is modeled to arise in the warm gas downstream of the 38 km s^{-1} shock.

To derive the shock conditions, we invoke the MHD C-shock models of Draine et al. (1983), Draine & Roberge (1984), and Roberge & Draine (1990). These models span a large parameter space: density, velocity, and magnetic field all affect the post-shock conditions. When applied to the Galactic center region, the difficulty is the potentially large magnetic field. Draine et al. (1983) present CO intensities only for models with standard magnetic field, $B = 100\ \mu\mathrm{G}(n/10^4\ \mathrm{cm}^{-3})^{0.5}$. The field strength has a tremendous impact on the postshock excitation; in general the peak temperature is proportional to the square of the magnetic field and square of the shock velocity. An increase in the field strength by a factor of 3 can reduce high-J line intensities as much as a factor of 100, while the peak J and its intensity remain approximately unchanged. Other high-excitation lines such as those of H_2O, H_2, and [O I] are similarly affected. The direct observational constraints on the field strength are not strong because the Zeeman measurements are difficult. It is known that within 3–4 pc of Sgr A* there are regions with B as large as 3 mG, although this does not pervade the region. In the CND itself, for example, there is no measurable field with an upper limit of 0.5 mG (Plante et al. 1995; Marshall et al. 1995). As these investigators point out, however, the large turbulent and orbital motions may distort and reverse the field such that the average measured field in a large (44″) beam may underestimate its local strength.

Using the published low magnetic field models, the general shape of the CO line intensity distribution, the peaking at $J \sim 8$, and the falling off toward higher J is reproduced for a range of density and velocity, from $n_{\mathrm{H}} \sim 10^4$ cm^{-3}, $v = 20$ km s^{-1} to $n_{\mathrm{H}} \sim 10^5$ cm^{-3}, $v = 13$ km s^{-1}. In all of these model cases, however, the transitions below the peak ($\sim J = 1$–5) are predicted to be brighter relative to the mid- and high-J transitions than is observed. This is likely due in part to the lower-J lines being optically thin in the observed region owing to the large velocity dispersion, relative to the models in which all of the lower-J CO lines are optically thick. A similar effect has been noted in considering the ground-state ($J = 1 \rightarrow 0$) HCN transition emission observed in the CND. The large velocity dispersion produces a low optical depth and reduces self-absorption, producing a high intensity per gas mass as compared with the more typical molecular clouds with less motion (see, e.g., Wright et al. 2001). Given this optical depth consideration, the higher density, lower velocity solution best reproduces the relative CO intensities, underpredicting the $J = 8/J = 3$ intensity ratio by a factor of only 2. Large magnetic fields are appealing because they allow a great deal of energy to be radiated in a fairly low excitation gas; this is the sort of situation that is required to reproduce CO luminosity that is comparable to or greater than the luminosity in [O I]. Given the CO lines, the observed and inferred [O I] intensity, and the published models of Draine et al. (1983), we conclude that a model with density of 10^4–10^5 cm^{-3} and velocity–magnetic field product of 10–20 km s^{-1} times 0.5–0.3 mG is the most likely description of the shock conditions in the central 2 pc.

In this scenario, the shock conditions that are exciting the mid-J CO are not the same as those that excite the near-IR H_2 lines. Gatley et al. (1986) have mapped a two-lobe structure in the H_2 $\nu = 1 \rightarrow 0$ $S(1)$ around Sgr A*, which is consistent with the shape of the CND, and as pointed out above, this emission has been found to be due to shock excitation (Tanaka et al.

1989). However, the low-velocity C-shocks that account for the observed CO emission would not include appreciable luminosity in the near-IR H_2 lines. These scenarios are not inconsistent; there are likely a variety of shock conditions around Sgr A*. Gatley et al. (1986) claim that the H_2 emission is due to shocks at the inner edge of the molecular disk due to mass outflow from Sgr A*. The CO-emitting shocks, on the other hand, arise from the dissipation of dynamical turbulence in the bulk of molecular rings.

5.2. *Turbulent Dissipation and Orbit Decay in the Central* 2 pc

We now turn to the energetics of the turbulent dissipation. Stone et al. (1998) and Mac Low (1999 and references therein) have studied the dissipation rate in MHD turbulence and find that the rate is comparable to that of a pure hydrodynamical turbulence and is essentially given by dimensional analysis. To get the correct coefficient, we rearrange equation (7) in Mac Low (1999) to express the energy output per mass of turbulent material as

$$\frac{L}{M} = 0.42\,\frac{v_{\rm rms}^3}{\Lambda_d} = 1.10\left(\frac{v_{\rm rms}}{25\ {\rm km\ s^{-1}}}\right)^3\left(\frac{1\ {\rm pc}}{\Lambda_d}\right)\ \frac{L_\odot}{M_\odot}, \quad (6)$$

where $v_{\rm rms}$ is the typical turbulent velocity and Λ_d is the size scale of the typical turbulent structures. The turbulent size scale should be comparable to or smaller than the smallest observed clump size, of order 0.1 pc according to the interferometric HCN measurements (also comparable to the Jeans length scale). We therefore adopt $\Lambda_d \sim 0.1$ pc. Taking a mid-range value from the above analysis, we apply $v_{\rm rms} = 15$ km s^{-1} to equation (6), yielding a power dissipated per unit mass of $(L/M)_{\rm turb} = 2.4$ in solar units. This is a reasonable match to the observed and inferred cooling rates in CO, [O I], and H_2. Note also that the adopted values for Λ_d and $v_{\rm rms}$ are broadly consistent with the 300 km s^{-1} pc^{-1} velocity gradient used in the LVG analysis: 15 km s^{-1}/0.1 pc $\sim$ 150 km s^{-1} pc^{-1}.

If the luminosity in the molecular lines is the result of turbulence in the steady state, then the orbit of the molecular material must be decaying. Differentiating the expression for Keplerian motion gives

$$\frac{dR}{dt} = \frac{2R^2}{GM}\frac{dE}{dt}, \quad (7)$$

where M is the enclosed mass and E represents the energy per mass of the molecular gas. For an orbit around $4 \times 10^6\ M_\odot$ at a distance of 1.5 pc, the observed luminosity-to-mass ratio corresponds to an orbit decay rate of 4×10^{-6} pc yr^{-1}. Thus, infall from the radius of the HCN ring ($R \sim 2$ pc) to the inner edge of the CND as traced in the far-IR ($R \sim 1.5$ pc) would require 1.2×10^5 yr, similar to the orbital timescale $\sim 9 \times 10^4$ yr. Thus, this gas is dissipating its orbital energy on an orbital timescale and cannot exist for more than a few orbits, or a few times 10^5 yr. This is not surprising if the material that forms the CND and other features derives from orbits with low angular momentum, and the CND itself represents the circularization of that material at a radius appropriate for its angular momentum.

Recent modeling has given some theoretical basis for the formation of the CND and streamers as the result of infalling clouds. Sanders (1998) produces an asymmetric elliptical structure, called a dispersion ring, by tidal disruption of a clumpy cloud incident on a point mass from 6.5 pc with angular momentum of a 1 pc radius circular orbit. After the material makes one or two passes (about 8×10^5 yr), the resulting debris is a circumnuclear structure that reproduces the kinematics of the HCN ring more accurately than any circular rotation scenario and hints at the same morphological structure.

Although the overall distribution is not symmetric, the innermost edge of the dispersion ring is elliptical and consistent with the observed far-IR morphology (L99). Throughout the simulation, the interior radius of the CND gradually decreases, the result of repeated collisions between clumps, which would certainly produce shocks and possibly trigger star formation. Whether the inner radius stabilizes or some of the gas eventually accretes onto the central mass depends on the details of the viscosity and the formation of stars. Sanders (1998) uses a very similar infalling cloud scenario to model the NA and the east-west bar, each independently. This is appealing, as there is convincing observational evidence that the NA is an infalling streamer produced in a collision between two clouds somewhere outside the CND (L99; Herter et al. 1989; J93). The NA is in an earlier stage of infall than the CND gas, roughly on its first passage, and has lower specific angular momentum, both of which make it more recognizable observationally. It is significant that the model can generate the same CND morphology and kinematics as traced with the far-IR and the HCN and provide a natural fit with the dynamically driven energetics we derive for the material around Sgr A*.

6. CONCLUSIONS

We present an 11″ spatial resolution map of the central 2 pc of the galaxy in the $J = 7 \rightarrow 6$ rotational transition of CO. An LVG analysis invoking all the available CO line intensities provides constraints on the conditions in the molecular gas. We find that warm, 200–300 K, moderate-density, $n \sim (5-7) \times 10^4$ cm^{-3}, molecular gas is abundant in the Galactic center, with total CO luminosity comparable to that of the atomic lines. The total mass of warm molecular material is at least 2000 $M_\odot$, slightly less than the total mass measured with cooler molecular gas tracers, but an order of magnitude more than the mass in photodissociated atomic gas. Morphologically and kinematically, the CO emission bears some resemblance to the CND as traced with HCN and the far-IR continuum, but also reveals noncircular turbulent motion. Heating with a central UV source is not capable of producing the observed CO luminosity, and we conclude that the primary energy source is dynamical. The observed spectral tracers are consistent with mechanical energy being dissipated into the gas in low-velocity (10–20 km s^{-1}) shocks with magnetic fields of 0.3–0.5 mG, and these values are consistent with other observational evidence. Our results support a scenario in which the CND and other features around Sgr A* are each in the process of forming from infalling molecular clouds with low angular momentum on timescales of 10^5 yr.

We thank Wayne Holland (currently at the UK ATC), Richard Prestage (currently at NRAO Green Bank), and the JCMT operators and technical staff for their help in making the commissioning run of SPIFI a success. We thank David Flower (Durham University) for providing the high-temperature CO-H_2 rate coefficients in advance of publication. C. M. B. acknowledges support from a Milliken Fellowship at Caltech. We thank an anonymous referee for several helpful comments on a draft of the manuscript.

REFERENCES

Balick, B., & Brown, R. L. 1974, ApJ, 194, 265
Becklin, E. E., Gatley, I., & Werner, M. W. 1982, ApJ, 258, 135
Becklin, E. E., & Neugebauer, G. 1968, ApJ, 151, 145
———. 1969, ApJ, 157, L31
Blake, G. A., Sutton, E. C., Masson, C. R., & Phillips, T. G. 1987, ApJ, 315, 621
Bradford, C. M., Stacey, G. J., Nikola, T., Bolatto, A. D., Jackson, J. M., Savage, M. L., & Davidson, J. A. 2003, ApJ, 586, 891
Bradford, C. M., Stacey, G. J., Swain, M. R., Nikola, T., Bolatto, A. D., Jackson, J. M., Savage, M. L., & Davidson, J. A. 2002, Appl. Opt., 41, 2561
Burton, M. G., Hollenbach, D. J., & Tielens, A. G. G. M. 1990, ApJ, 365, 620
Draine, B. T., & Roberge, W. G. 1984, ApJ, 282, 491
Draine, B. T., Roberge, W. G., & Dalgarno, A. 1983, ApJ, 264, 485
Ekers, R. D., van Gorkom, J. H., Schwarz, U. J., & Goss, W. M. 1983, A&A, 122, 143
Evans, N. J., Lacy, J. H., & Carr, J. S. 1991, ApJ, 383, 674
Flower, D. R. 2001, J. Phys. B, 34, 2731
Flower, D. R., & Launay, J. M. 1985, MNRAS, 214, 271
Gatley, I., & Becklin, E. E. 1981, in IAU Symp. 96, Infrared Astronomy, ed. C. G. Wynn-Williams & D. P. Cruikshank (Dordrecht: Reidel), 281
Gatley, I., Becklin, E. E. Werner, M. W., & Wynn-Williams, C. G. 1977, ApJ, 216, 277
Gatley, I., Jones, T. J., Hyland, A. R., Wade, R., Geballe, T. R., & Krisciunas, K. 1986, MNRAS, 222, 299
Genzel, R., Stacey, G. J., Harris, A. I., Townes, C. H., Geis, N., Graf, U. U., Poglitsch, A., & Stutzki, J. 1990, ApJ, 356, 160
Genzel, R., Watson, D. M., Crawford, M. K., & Townes, C. H. 1985, ApJ, 297, 766
Ghez, A., Becklin, E., Duchjne, G., Hornstein, S., Morris, M., Salim, S., & Tanner, A. 2003, Astron. Nachr., 324, 527
Goldreich, P., & Kwan, J. 1974, ApJ, 189, 441
Goldsmith, P., & Langer, W. D. 1978, ApJ, 222, 881
Güsten, R., Genzel, R., Wright, M. C. H., Jaffe, D. T., Stutzki, J., & Harris, A. 1987, ApJ, 318, 124
Harris, A. I., Jaffe, D. T., Silber, M., & Genzel, R. 1985, ApJ, 294, L93
Herrmann, F., Madden, S. C., Nikola, T., Poglitsch, A., Timmermann, R., Geis, N., Townes, C. H., & Stacey, G. J. 1997, ApJ, 481, 343
Herrnstein, R., & Ho, P. T. P. 2002, ApJ, 579, L83
———. 2005, ApJ, 620, 287
Herter, T., Gull, G. E., Megeath, S. T., Rowlands, N., & Houck, J. R. 1989, ApJ, 343, 696
Hoffman, W. R., Frederick, C. L., & Emery, R. J. 1971, ApJ, 170, L89
Huettemeister, S., Dahmen, G., Mauersberger, R., Henkel, C., Wilson, T. L., & Martin-Pintado, J. 1998, A&A, 334, 646
Huettemeister, S., Wilson, T. L., Bania, T. M., & Martin-Pintado, J. 1993, A&A, 280, 255
Jackson, J. M., Geis, N., Genzel, R., Harris, A. I., Madden, S., Poglitsch, A., Stacey, G. J., & Townes, C. H. 1993, ApJ, 402, 173 (J93)
Kaufman, M. J., Wolfire, M. G., Hollenbach, D. J., & Luhman, M. L. 1999, ApJ, 527, 795
Koester, B., Stoerzer, H., Stutzki, J., & Sternberg, A. 1994, A&A, 284, 545
Lacy, J. H., Townes, C. H., Geballe, T. R., & Hollenbach, D. J. 1980, ApJ, 241, 132
Latvakoski, H. M., Stacey, G. J., Gull, G. E., & Hayward, T. L. 1999, ApJ, 511, 761 (L99)
Le Bourlot, J., Pineau des Forets, G., & Flower, D. D. R. 1999, MNRAS, 305, 802
Leung, C. M., Herbst, E., & Huebner, W. F. 1984, ApJS, 56, 231
Lo, K. Y., & Claussen, M. J. 1983, Nature, 306, 647
Lugten, J. B. 1987, Ph.D. thesis, Univ. California, Berkeley
Mac Low, M.-M. 1999, ApJ, 524, 169
Marshall, J., Lasenby, A. N., & Yusef-Zadeh, F. 1995, MNRAS, 274, 519
McKee, C. F., Storey, J. W. V., Watson, D. M., & Green, S. 1982, ApJ, 259, 647
McNamara, D. H., Madsen, J. B., Barnes, J., & Ericksen, B. F. 2000, PASP, 112, 202
Meixner, M., & Tielens, A. G. G. M. 1993, ApJ, 405, 216
Moneti, A., Cernicharo, J., & Pardo, J. R. 2001, ApJ, 549, L203
Neufeld, D. A., Lepp, S., & Melnick, G. J. 1995, ApJS, 100, 132
Oort, J. H., & Rougoor, G. W. 1960, MNRAS, 121, 171
Plante, R. L., Lo, K. Y., & Crutcher, R. M. 1995, ApJ, 445, L113
Roberge, W. G., & Draine, B. T. 1990, ApJ, 350, 700
Roberts, D. A., Yusef-Zadeh, F., & Goss, W. M. 1996, ApJ, 459, 627
Rodríguez-Fernández, N. J., Martín-Pintado, J., de Vicente, P., Fuente, A., Hüttemeister, S., Wilson, T. L., & Kunze, D. 2000, A&A, 356, 695
Rodríguez-Fernández, N. J., Martín-Pintado, J., Fuente, A., de Vicente, P., Wilson, T. L., & Hüttemeister, S. 2001, A&A, 365, 174
Rodríguez-Fernández, N. J., Martín-Pintado, J., Fuente, A., & Wilson, T. L. 2004, A&A, 427, 217
Rudy, D. J., Muhleman, D. O., Berge, G. L., Jakosky, B. M., & Christensen, P. R. 1987, Icarus, 71, 159
Sanders, R. H. 1998, MNRAS, 294, 35
Sandqvist, Aa., et al. 2003, A&A, 402, L63
Savage, B. D., & Sternbach, K. R. 1996, ARA&A, 34, 279
Schinke, R., Engel, V., Buck, U., Meyer, H., & Diercksen, G. H. F. 1985, ApJ, 299, 939
Schmid-Burgk, J., et al. 1989, A&A, 215, 150
Schödel, R., Ott, T., Genzel, R., Eckart, A., Mouawad, N., & Alexander, T. 2003, ApJ, 596, 1015
Schwarz, U. J., Bregman, J. D., & van Gorkom, J. H. 1989, A&A, 215, 33
Scoville, N. Z., & Solomon, P. M. 1974, ApJ, 187, L67
Serabyn, E., Güsten, R., Walmsley, C. M., Wink, J. E., & Zylka, R. 1986, A&A, 169, 85
Stacey, G. J., Jaffe, D., Geis, N., Genzel, R., Harris, A., Poglitsch, A., & Townes, C. H. 1993, ApJ, 404, 219
Stone, J. M., Ostriker, E. C., & Gammie, C. F. 1998, ApJ, 508, L99
Sutton, E. C., Danchi, W. C., Jaminet, P. A., & Masson, C. R. 1990, ApJ, 348, 503
Tanaka, M., Hasegawa, T., Hayashi, S., Brand, P. W. J. L., & Gatley, I. 1989, ApJ, 336, 207
Tielens, A. G. G. M., & Hollenbach, D. 1985, ApJ, 291, 722
Viscuso, P. J., & Chernoff, D. F. 1988, ApJ, 327, 364
Vollmer, B., & Duschl, W. J. 2002, A&A, 388, 128
Watson, D. M., Genzel, R., Townes, C. H., & Storey, J. W. V. 1985, ApJ, 298, 316
White, G. J., Smith, H. A., Stacey, G. J., Fischer, J., Spinoglio, L., Baluteau, J.-P., Cernicharo, J., & Bradford, C. M. 1999, in The Universe as Seen by *ISO*, ed. P. Cox & M. F. Kessler (ESA-SP 427; Noordwijk: ESA), 787
Wilson, T. L., Ruf, K., Walmsley, C. M., Martin, R. N., Batrla, W., & Pauls, T. A. 1982, A&A, 115, 185
Wright, E. L. 1976, ApJ, 210, 250
Wright, M. C. H., Coil, A., McGary, R. S., Ho, P. T. H., & Harris, A. I. 2001, ApJ, 551, 254
Wright, M. C. H., Marr, J. M., & Backer, D. C. 1989, in IAU Symp. 136, The Center of the Galaxy, ed. M. Morris (Dordrecht: Kluwer), 407